

Synthesis and stability of $\text{Fe}_3^{2+}\text{Fe}_2^{3+}\text{Si}_3\text{O}_{12}$ garnet and phase relations with $\text{Fe}_3\text{Al}_2\text{Si}_3\text{O}_{12}$ – $\text{Fe}_3^{2+}\text{Fe}_2^{3+}\text{Si}_3\text{O}_{12}$ solutions

ALAN B. WOODLAND, HUGH ST.C. O'NEILL

Bayerisches Geoinstitut, Postfach 10 12 51, D-95440 Bayreuth, Germany

ABSTRACT

Garnets containing both Fe^{2+} and Fe^{3+} are potentially useful monitors of f_{O_2} in metamorphic rocks and garnet peridotites of the mantle. However, little is known about the properties or stability of such garnets. We have synthesized end-member $\text{Fe}_3^{2+}\text{Fe}_2^{3+}\text{Si}_3\text{O}_{12}$ garnet and garnet along the almandine ($\text{Fe}_3^{2+}\text{Al}_2\text{Si}_3\text{O}_{12}$)– $\text{Fe}_3^{2+}\text{Fe}_2^{3+}\text{Si}_3\text{O}_{12}$ join, where Al and Fe^{3+} mix on the octahedral sites. The experiments were performed with a series of glasses and slags with a fixed ratio of $\text{Fe}^{3+}/\text{Fe}_{\text{tot}}$ in a piston cylinder apparatus and a multianvil press using Ag as the capsule material. The extent of Fe^{3+} substitution for Al is strongly pressure dependent. At 1100 °C, the maximum $\text{Fe}_3^{2+}\text{Fe}_2^{3+}\text{Si}_3\text{O}_{12}$ content is 13, 43, and 75 mol% at 2.7, 6.5, and 8.0 GPa, respectively. The end-member ferrous-ferric garnet is only stable at pressures above ≈ 9.3 GPa. However, skiaegite becomes unstable at higher pressures of even < 13.0 GPa. Mössbauer spectroscopy confirms that Fe^{2+} and Fe^{3+} are restricted to the dodecahedral and octahedral sites, respectively. Molar volumes of $\text{Fe}_3^{2+}\text{Fe}_2^{3+}\text{Si}_3\text{O}_{12}$ and almandine are $121.44 \pm 0.01 \text{ cm}^3$ [$a_0 = 11.7278(6) \text{ \AA}$] and $115.23 \pm 0.01 \text{ cm}^3$, [$a_0 = 11.5244(4) \text{ \AA}$] and vary linearly across the binary join.

At 1100 °C, the equilibrium garnet solid solutions coexist with fayalite + spinel + quartz at $P < 1.6$ GPa, with spinel + $\text{Fe}_2\text{Si}_2\text{O}_6$ + quartz or coesite at $1.6 < P < 5.0$ GPa, and with Si-rich spinel + coesite or stishovite above 5.0 GPa. The coexisting spinel and pyroxene are very Al poor, indicating that Al is strongly partitioned into the garnet. Based upon Al– Fe^{3+} exchange between garnet and spinel, a $\Delta_r G_{1,1373}^\circ = -2975.2 \pm 3.0 \text{ kJ/mol}$ is obtained for $\text{Fe}_3^{2+}\text{Fe}_2^{3+}\text{Si}_3\text{O}_{12}$, assuming ideal mixing in the garnet. The spinel becomes increasingly $\text{Fe}_2\text{Si}_2\text{O}_6$ -rich with increasing pressure such that the $\text{Fe}^{3+}/\text{Fe}_{\text{tot}}$ of the end-member $\text{Fe}_3^{2+}\text{Fe}_2^{3+}\text{Si}_3\text{O}_{12}$ garnet and coexisting spinel are nearly the same.

INTRODUCTION

Garnet is an important phase in the Earth's lower crust and mantle. Its common occurrence has led to the use of garnet-bearing equilibria as indicators of temperature and pressure (e.g., O'Neill and Wood, 1979; Bohlen et al., 1983b; Hackler and Wood, 1989). The compositions of such garnets can generally be expressed in terms of three main components: pyrope ($\text{Mg}_3\text{Al}_2\text{Si}_3\text{O}_{12}$), grossular ($\text{Ca}_3\text{Al}_2\text{Si}_3\text{O}_{12}$), and almandine ($\text{Fe}_3^{2+}\text{Al}_2\text{Si}_3\text{O}_{12}$). The presence of Fe implies that the stability of garnet is controlled in part by f_{O_2} . The incorporation of Fe^{3+} in aluminous garnet has several important petrologic implications. Garnet-bearing reactions could be potential monitors of f_{O_2} for garnet peridotites and eclogites (Luth et al., 1990). Garnet could be an important sink for Fe^{3+} at depths $> \approx 60$ km, where Fe^{3+} -bearing aluminous spinel becomes unstable (Wood et al., 1990). The incorporation of Fe^{3+} in majorite garnet [$(\text{Mg}, \text{Fe}^{2+})_4\text{Si}_4\text{O}_{12}$] could strongly influence the f_{O_2} in the transition zone of the mantle (O'Neill et al., 1993). The presence of Fe^{3+} in garnet can also have a significant effect on temperature and pressure estimates, especially those based upon Mg–Fe exchange equilibria (Luth et al., 1990).

Woodland and Wood (1989) derived the free energy of

formation of almandine from the reaction involving silimanite, quartz, and metallic Fe. Their study revealed that small amounts of Fe^{3+} could substitute for Al and that these small quantities had an apparent effect on garnet stability. Minor substitution of Fe^{3+} for Al in almandine was also reported by Geiger et al. (1987). The recent study of mantle-derived garnets by Luth et al. (1990) showed that up to 12% of the Fe can be in the ferric state. Their attempt at using the Fe^{3+} content of the garnets to determine f_{O_2} was hampered, however, by the absence of thermochemical data on the mixing properties of Fe^{3+} in garnet. Mössbauer spectroscopy on these and other garnets (Amthauer et al., 1976) indicates that Fe^{3+} usually resides on the octahedral sites. Therefore, the Fe^{3+} -bearing components to consider are skiaegite ($\text{Fe}_3^{2+}\text{Fe}_2^{3+}\text{Si}_3\text{O}_{12}$), khoharite ($\text{Mg}_3\text{Fe}_2^{3+}\text{Si}_3\text{O}_{12}$), and andradite ($\text{Ca}_3\text{Fe}_2^{3+}\text{Si}_3\text{O}_{12}$). Thermochemical data for all three components are necessary in order to account for the reciprocal solid-solution effects in natural multicomponent $(\text{Mg}, \text{Fe}^{2+}, \text{Ca})_3(\text{Al}, \text{Cr}, \text{Fe}^{3+})_2\text{Si}_3\text{O}_{12}$ garnet solid solutions. $\text{Fe}_3^{2+}\text{Fe}_2^{3+}\text{Si}_3\text{O}_{12}$ is the obvious choice for a study of garnets that contain both Fe^{2+} and Fe^{3+} , since cation mixing can be limited to one site. In $\text{Fe}_3\text{Al}_2\text{Si}_3\text{O}_{12}$ – $\text{Fe}_3^{2+}\text{Fe}_2^{3+}\text{Si}_3\text{O}_{12}$ solutions, Fe^{3+} substitutes for Al on the octahedral sites. Although skiaegite,

the name for $\text{Fe}_2^{3+}\text{Fe}_2^{3+}\text{Si}_3\text{O}_{12}$, has been discredited as a proper mineral name, we retain the use of the term skia-gite (ski) to refer to an end-member component that may occur in complex garnet solid solutions.

Garnet with significant skia-gite content has been synthesized by Schreyer and Baller (1980) and Lattard and Schreyer (1983) in the Mn-Fe-Si-O system. Synthesis of the pure skia-gite end-member was first reported by Karpinskaya et al. (1982), based upon several X-ray reflections that could not be assigned to the other phases present in their experimental products. Their experiments suggest that garnet could be a stable phase in the system $\text{FeO-Fe}_2\text{O}_3\text{-SiO}_2$ at high pressure.

The purpose of this study was to determine the maximum extent of Fe^{3+} substitution for Al in garnet by the synthesis of almandine-skia-gite solid solutions. The synthesis of the skia-gite end-member was also important to verify the results of Karpinskaya et al. (1982) and to characterize this end-member garnet. In addition, we set out to establish the phase relations between garnet and spinel, olivine, and pyroxene in the system $\text{FeO-FeO}_{1.5}\text{-AlO}_{1.5}\text{-SiO}_2$ and to derive some thermodynamic properties of skia-gite and almandine-skia-gite solutions.

EXPERIMENTAL METHODS

Apparatus and experimental techniques

Experiments in the pressure range of 1.5–5.0 GPa were conducted in a piston cylinder apparatus. Talc-Pyrex pressure cells with diameters of 1.905 and 1.270 cm were used, depending on the desired pressure. The temperature was controlled by means of Pt-Pt₉₀Rh₁₀ thermocouples with no correction for the effect of pressure on the emf. The experiments employed the piston-in technique. The pressure was calibrated in the 1.905-cm cells from (1) the olivine-spinel transition in Mg_2GeO_4 (Ross and Navrotsky, 1987), (2) the albite + jadeite + quartz equilibrium (Holland, 1980), (3) the ferrosilite + fayalite + quartz equilibrium (Bohlen et al., 1980), and (4) the pyroxene-garnet transition in CaGeO_3 (Ross et al., 1986). The pressure calibration for the 1.270-cm cells was determined from (1) the quartz-coesite transition (Bohlen and Boettcher, 1982), and (2) the olivine-spinel transition in Mg_2GeO_4 . The uncertainty in pressure is estimated to be ≈ 0.1 GPa, based upon the width of our calibration brackets. The duration of the experiments was mostly between 40 and 100 h. The starting materials were ground under acetone and packed in 5-mm Ag capsules with walls 0.5 mm thick and sealed by friction-fitting lids hammered in place. The choice of Ag as the capsule material was based on the premise that Ag would not absorb any Fe (Massalski et al., 1986) and that Ag is one of the metals more impervious to H_2 . This is an important consideration, since diffusion of H_2 into the capsule during the experiment could change the O content of the solid and, therefore, the $\text{Fe}^{3+}/\text{Fe}_{\text{tot}}$ ratio of the sample. Experiments involving almandine-rich compositions ($\leq \text{ski}_{0.5}$) were conducted in 6-mm graphite capsules. Most experiments were conducted at 1100 °C; however, below ≈ 3.0 GPa

the experiments were at a somewhat lower temperature to avoid melting of the Ag capsules. Several experiments at low pressure were performed with Au capsules in order to reach 1100 °C without melting the capsule material. It is possible that some Fe loss to the capsule could have occurred in these experiments, since there is significant Fe solubility in Au.

Experiments at 5.5–10.0 GPa were conducted in the Sumitomo 1200 multianvil press at the Bayerisches Geoinstitut using Toshiba F grade tungsten carbide cubes with an 11-mm truncated edge. The pressure cells were Cr_2O_3 -doped MgO octahedra, 18 mm on an edge, heated by a graphite resistance heater. Temperature was monitored by axially inserted Pt-Pt₉₀Rh₁₀ thermocouples with no correction made for the pressure effect on emf. The pressure was calibrated at room temperature using the transitions in Bi (I-II, III-V) and at 1000 and 1450 °C using the transitions (1) quartz-coesite (Bohlen and Boettcher, 1982), (2) coesite-stishovite (Yagi and Akimoto, 1976), and (3) fayalite- γ spinel (Yagi et al., 1987). The accuracy in the pressure is estimated to be ± 0.3 GPa, based on the width of the reversal brackets and repeated checks of these reactions. The capsules for the multianvil press experiments were made from 1.7-mm Ag tubing. The ends were sealed by the insertion of an Ag disk, followed by crimping and hammering, which produced a cold weld. The duration of the multianvil experiments was 10–14.5 h.

Starting materials

Since control of f_{O_2} (e.g., by the double capsule technique) is impractical in the multianvil experiments, we chose instead to rely on a closed system approach for experiments in both apparatus by analysis of the $\text{Fe}^{3+}/\text{Fe}_{\text{tot}}$ ratio in the products. In order to obtain starting materials with the correct stoichiometry for the garnet solid solutions, the $\text{Fe}^{3+}/\text{Fe}_{\text{tot}}$ ratio must be set. The $\text{Fe}^{3+}/\text{Fe}_{\text{tot}}$ ratio varies from 0.0 in almandine (only Fe^{2+} is present) to 0.40 for pure skia-gite. This ratio was established by using mixtures of fayalite, quartz, and an appropriate hercynite-magnetite solid solution to achieve the correct $\text{Fe}^{3+}/\text{Fe}_{\text{tot}}$. Although this proved effective for the synthesis of the almandine end-member using pure hercynite, the syntheses of the solid solutions were not successful. In the experiments with alm-ski solutions, almandine-rich garnet would nucleate on and mantle the spinel, effectively stopping the reaction from proceeding to completion. In addition, local Al-Fe exchange would occur between the garnet and the spinel, yielding a very almandine-rich garnet and magnetite-rich rims on the spinel grains. To circumvent this problem, glasses or slags were prepared by melting stoichiometric amounts of Fe_2O_3 , Al_2O_3 , and SiO_2 at 1500 °C. The correct $\text{Fe}^{3+}/\text{Fe}_{\text{tot}}$ ratio was achieved by controlling the f_{O_2} of the furnace atmosphere using CO-CO_2 or Ar-O_2 gas mixes. The value of f_{O_2} that would yield the desired $\text{Fe}^{3+}/\text{Fe}_{\text{tot}}$ was estimated from Kress and Carmichael (1988) and from Figure 6902 in Roth et al. (1987, p. 454–456). Nonmagnetic glasses

TABLE 1. Experimental results

Expt.	T (°C)	P (GPa)	t (h)	Intended comp.	Phases produced	Probe comp.	Cell edge (Å)		Spinel comp.		
							Garnet	Spinel	Fe ₂ Si-O ₄	Mt	Hc
al5*	1100	1.5	6	ski ₀₀	gt	ski ₀₀	11.531(2)				
aw1***	1200	2.0	42	ski ₀₀	gt + q + Fe	ski ₀₀	11.5285(2)				
aw6***	1200	1.9	44	ski ₀₀	gt + q + Fe	ski ₀₀	11.5285(2)				
aw14***	1100	1.7	24	ski ₀₀	gt	ski ₀₂	11.5312(8)				
aw35**	1000	2.0	168	ski ₀₀	gt + opx + q	ski ₀₀	11.5292(7)				
aw43**	1080	3.2	41	ski ₀₀	gt + opx	ski ₀₂	11.5333(2)				
aw18*	1200	3.0	24	ski ₀₅	gt + q	ski ₀₂	11.5299(5)				
aw25	1080	2.7	46	ski ₁₀	gt + q	ski ₀₈	11.5400(6)				
aw26	1080	2.7	96	ski ₁₀	gt + q	ski ₀₈	11.5390(9)				
aw30	1080	2.7	97	ski ₁₀	gt + q	ski ₀₇	11.5408(3)				
aw31	1030	1.9	96	ski ₁₀	gt + q + sp	ski ₀₉	11.5380(2)	8.369(1)	4	87	9.0
aw45	1080	2.7	101	ski ₁₀	gt + q	ski ₀₈	11.5405(2)				
aw21	1100	3.0	40	ski ₁₅	gt + sp + q + opx	ski ₁₂	11.5494(2)	8.373(1)	7	88	5.3
aw29	1080	2.7	89	ski ₁₅	gt + sp + q + opx	ski ₁₂	11.5495(2)	8.374(1)	7	88	4.8
aw37	1100	4.0	96	ski ₁₅	gt	ski ₁₅	11.5546(4)				
aw41	1100	3.5	89.5	ski ₁₅	gt + sp	ski ₁₇	11.5594(2)	8.377(1)			
aw48†	1100	1.7	116.5	ski ₁₅	gt + sp + q + opx	ski ₁₀	11.5426(5)	8.360(1)	4	83	13.0
aw15*	1200	3.0	95	ski ₂₀	gt + sp + q + opx	ski ₀₃	11.5336(5)				
aw21	1100	3.0	40	ski ₂₀	gt + sp + q + opx	ski ₁₃	11.5522(6)	8.371(1)	7	88	5.3
aw26	1080	2.7	96	ski ₂₀	gt + opx + fa	ski ₁₁	11.5477(7)				
aw29	1080	2.7	89	ski ₂₀	gt + sp + q + opx	ski ₁₂	11.5501(2)	8.374(1)	8	87	5.0
aw32	1080	2.7	90	ski ₂₀	gt + sp + q + opx	ski ₁₃	11.5507(10)		8	87	5.2
aw34†	1180	2.7	49	ski ₂₀	gt + opx + q	ski ₀₉	11.5430(4)				
aw37	1100	4.0	96	ski ₂₀	gt	ski ₂₁	11.5571(5)				
aw23	1080	2.7	47	ski ₃₀	gt + sp + q + opx	ski ₁₃	11.5489(2)	8.368(1)	10	85	5.2
aw38	1100	4.4	70	ski ₃₀	gt + sp + coe	ski ₁₄	11.5647(5)	8.373(1)	10	87	3.0
aw47	1100	4.8	46	ski ₃₀	gt + sp + q + opx	ski ₃₀	11.5837(7)				
uhp458	1100	6.0	11	ski ₃₀	gt + coe + sp	ski ₂₉	11.5777(7)	8.359(1)			
uhp541	1100	6.5	12	ski ₄₀	gt	ski ₄₁	11.6061(9)				
uhp541	1100	6.5	12	ski ₅₀	gt + sp + opx	ski ₄₄	11.6123(8)				
uhp627	1100	7.0	12.5	ski ₅₀	gt + coe + sp	ski ₅₀	11.6273(3)				
uhp532	1100	8.0	12	ski ₇₀	gt + sp + cpx	ski ₇₀	11.6615(4)		63	36	0.8
uhp497	1100	9.0	12	ski ₈₀	gt + hem + coe	ski ₇₉	11.6841(7)				
uhp532	1100	8.0	12	ski ₈₀	gt + coe + sp	ski ₇₅	11.6735(4)	8.3242(8)	46	54	0.4
uhp610	1100	8.5	12	ski ₈₀	gt + sp + coe	ski ₇₆	11.6818(3)	8.3252(15)	44	56	0.3
uhp589	1100	9.0	12	ski ₉₀	gt + sp + hem + coe	ski ₇₇	11.6840(4)	8.3523(4)			
uhp598	1100	9.5	14	ski ₉₀	gt + sp + hem + coe	ski ₉₀	11.7076(7)				
uhp524	1100	9.0	11	ski ₁₀₀	gt + sp + coe	ski ₈₂	11.6903(7)	8.3153(9)	45	55	0.2
uhp548	1100	10.0	12	ski ₁₀₀	sp + gt + st	ski ₁₀₀	11.7286(10)	8.3187(2)	39	61	
uhp548	1100	10.0	12	ski ₁₀₀	sp + gt + st	ski ₁₀₀	11.7273(4)	8.3133(3)	45	55	
uhp598	1100	9.5	14	ski ₁₀₀ ‡	sp + coe + hem + gt	ski ₁₀₀	11.726(20)	8.3187(10)	43	57	
uhp666**	1100	9.3	12.5	ski ₁₀₀ ‡	sp + coe + gt + (px)	ski ₁₀₀	11.7250(15)	8.3224(2)	36	64	
uhp693**	1100	10.5	11.6	ski ₁₀₀ ‡	sp + gt + st	ski ₉₅	11.7163(5)	8.2981(14)			
uhp702**	1100	9.7	12.5	ski ₁₀₀ ‡	gt + st + sp	ski ₁₀₀	11.7272(7)				
uhp636**	1100	10.0	12.5	ski ₉₀ -fm ₄₀	gt + sp + st + (px)	ski ₉₈	11.7254(4)	8.2629(6)	76	24	
uhp693**	1100	10.5	11.6	ski ₉₀ -fm ₄₀	sp + st + gt	ski ₉₈	11.7126(8)	8.2649(8)	74	26	

Reequilibration experiments

Expt.	T (°C)	P (GPa)	t (h)	Starting comp.	Phases produced	Probe comp.	Cell edge (Å)		Spinel comp.		
							Garnet	Spinel	Fe ₂ Si-O ₄	Mt	Hc
aw45	1080	2.7	101	ski ₃₀ r	2gt + sp + opx + q	ski ₁₃	11.5510(10)	8.3745(2)	10	85	5.2
uhp642	1100	5.5	13.5	ski ₅₀ r	2gt + sp + coe + opx	ski ₃₃	11.5909(2)	8.370(3)	20	78	1.8
uhp627	1100	7.0	12.5	ski ₉₀ r	2gt + sp + coe + opx	ski ₅₉	11.6430(12)	8.347(3)	32	68	0.9
aw69	1100	4.1	115	ski ₁₃ r	gt + px + sp + coe	ski ₁₉					
uhp835	1100	6.0	14.5	ski ₂₁ r	gt + px + sp + coe	ski ₃₅					

Note: (px) = unreacted starting material.

* Used graphite capsule.

** Oxide mix.

† Used Au capsule.

‡ Garnet seed added.

were obtained up to compositions of 70 mol% almandine and 30 mol% skiagite (ski₃₀). However, at more Fe-rich compositions, quenching a glass became increasingly difficult, and a magnetic vitreous slag resulted. The Fe³⁺/

Fe_{tot} ratios of the glasses were checked by wet chemistry and were found to be within 10% of the nominal values. The glasses were also checked by Mössbauer spectroscopy. The resulting Fe³⁺/Fe_{tot} values were found to be

sensitive to the scheme used for fitting the spectra, but the range in values obtained was in agreement with the nominal ratio. The slags were not checked by either method because of the difficulty in completely dissolving oxide phases without causing oxidation and therefore spuriously high Fe^{3+} contents (Lucas et al., 1989) and because the presence of multiple phases would make any Mössbauer spectrum virtually impossible to interpret in a quantitative fashion. Since several of the slag starting materials produced homogeneous garnets either as a single phase or with only a trace of additional phases, the actual $\text{Fe}^{3+}/\text{Fe}_{\text{tot}}$ of the slags must have been close to the intended values (see below).

Several starting materials were used in experiments in the $\text{FeO-FeO}_{1.5}\text{-SiO}_2$ subsystem. Slags were synthesized in the manner described above. We also used two mineral mixes, ferrosilite + hematite and magnetite + fayalite + SiO_2 . The ferrosilite was synthesized from a mixture of fayalite and quartz in a piston cylinder apparatus at 1000 °C and 1.8 GPa. It was then ground together with hematite to produce a skiaigite bulk composition. A stoichiometric mixture of fayalite, magnetite, and either very high purity silica glass or SiO_2 produced from gel was also used. These mixtures were less successful in terms of yield, apparently owing to the sluggishness of reaction between SiO_2 and spinel.

Experimental products and analytical methods

The products were analyzed by X-ray diffraction, electron microprobe, and Mössbauer spectroscopy. The experimental conditions and the phases produced are listed in Table 1. The cell edges of the garnets were determined from the average of at least ten peaks above $60^\circ 2\theta$ using Ge monochromated $\text{CoK}\alpha_1$ radiation and NBS Si metal as an internal standard (STOE STADIP focusing diffractometer in transmission mode). Phase compositions were determined using a Cameca Camebax SX50 microprobe in wavelength-dispersive mode with a 15-kV accelerating voltage and a 15-nA beam current. The standards were Fe_2O_3 for Fe, spinel for Al, and either andradite or orthoclase for Si. The raw counts were recalculated using the PAP correction procedure. Garnet compositions were calculated assuming ideal stoichiometry of 8 cations pfu and charge balance.

Resonant absorption spectra were collected at 298 K with a Mössbauer spectrometer operating in constant acceleration mode and a ≈ 50 mCi ^{57}Co in Rh source. The velocity ramp was ± 5 mm/s. Mirror-image spectra were collected over 512 channels and calibrated with respect to α Fe at room temperature. The samples were prepared so that the Fe concentration was between 3 and 5 mg/cm² to avoid effects from saturation. The spectra were fitted using the PC-MOS software obtained from CMTE Elektronik, Auenstraße 15, D-85521 Riemerling, Germany. Some spectra were also fitted using the Mossfit program (see Luth et al., 1990) and were found to give the same hyperfine parameters and area ratios within the uncertainties of ± 0.01 mm/s and ± 0.01 , respectively.

RESULTS AND DISCUSSION

Garnet occurs as a single phase or coexists with one or more additional phases. The results of the individual experiments are summarized in Table 1. All the garnets are optically isotropic. Under oils the almandine-rich samples with compositions ≤ 5 mol% skiaigite are greenish. With increasing Fe^{3+} content, the garnets become pinkish ($\approx X_{\text{ski}} \leq 30$) and then take on a dark red-brown color. The skiaigite end-member is dark red-brown. The grain size is variable, with some samples having euhedral crystals up to 150 μm across. Other samples have much finer grained garnets, on the order of 5–30 μm . The grain size of the coexisting phases is often much smaller than that of the garnet. In some instances the nongarnet phases are < 3 μm across, precluding quantitative microprobe analysis.

Garnet composition

The almandine mole fraction was determined from the Al content as measured by electron microprobe, and the Fe^{3+} content was then calculated assuming ideal stoichiometry. Representative analyses of the garnets and associated phases are given in Table 2. The garnets in the experiments were quite homogeneous, generally yielding standard deviations of ≤ 2 mol%, corresponding to uncertainties in the calculated $\text{Fe}^{3+}/\text{Fe}_{\text{tot}}$ of ≤ 0.013 . However, the presence of both Fe^{2+} and Fe^{3+} adds to analytical uncertainty. For a garnet to lie on the almandine-skiaigite binary also requires that Fe^{2+} and Fe^{3+} be restricted to the dodecahedral and octahedral sites, respectively. Otherwise, some other garnet component such as $\text{Fe}_4^{2+}\text{Si}_4\text{O}_{12}$ must be considered.

To address this problem, Mössbauer spectra were collected from samples that either were single phase or contained only a trace of additional phases. The resultant room-temperature hyperfine parameters are listed in Table 3. Representative room-temperature Mössbauer spectra of four garnet samples with increasing Fe^{3+} content are presented in Figure 1a–1d. The most obvious features are the two doublets with distinctive line positions. The doublet with a large quadrupole splitting (QS) of ≈ 3.5 mm/s and an isomer shift (IS) of 1.3 mm/s is characteristic of Fe^{2+} in dodecahedral coordination (Amthauer et al., 1976). No statistically significant asymmetry is apparent between the low and high velocity peaks, as is often observed in garnets (e.g., Luth et al., 1990; Amthauer et al., 1976). When the two peaks are fitted separately rather than as a constrained doublet, the peak widths are identical within the resolution of the spectra. The full peak widths at half maximum (FWHM) for the $^{57}\text{Fe}^{2+}$ were 0.23–0.29 mm/s (Table 3). The other doublet, with a QS of 0.20–0.25 mm/s and IS of 0.31–0.36 mm/s, grows in relative intensity with increasing skiaigite content and can therefore be assigned to Fe^{3+} . The coordination of the Fe^{3+} can be deduced by comparison with the ranges in hyperfine parameters for $^{60}\text{Fe}^{3+}$ and $^{49}\text{Fe}^{3+}$ in garnet samples given by Amthauer et al. (1976): $^{60}\text{Fe}^{3+}$, IS =

TABLE 2. Representative microprobe analyses of synthesized garnet samples and associated phases

Expt. Phase	aw1 (ski ₁₀) Gt	aw6 (ski ₁₀) Gt	aw14 (ski ₁₀) Gt	aw43 (ski ₁₀) Gt	aw18 (ski ₁₀) Gt	aw25 (ski ₁₀) Gt
Al ₂ O ₃	20.43	20.33	20.06	19.90	19.88	18.89
FeO _{tot}	43.48	43.51	43.57	43.72	43.20	45.65
SiO ₂	35.91	35.85	35.90	35.64	35.58	36.42
Total	99.82	99.69	99.53	99.26	98.66	100.96
Structural formula						
Al	1.999	1.993	1.971	1.962	1.970	1.839
Fe ²⁺	2.982	2.981	2.992	2.981	2.992	3.008
Fe ³⁺	0.038	0.044	0.045	0.077	0.046	0.145
Si	2.982	2.981	2.992	2.981	2.992	3.008
Expt. Phase	aw26 (ski ₁₀) Gt	aw30 (ski ₁₀) Gt	aw31 (ski ₁₀) Gt	aw31 (ski ₁₀) Sp	aw45 (ski ₁₀) Gt	aw21 (ski ₁₅) Gt
Al ₂ O ₃	18.75	19.11	18.50	4.32	18.66	17.56
FeO _{tot}	44.64	45.49	45.13	88.47	45.51	46.41
SiO ₂	36.39	36.29	36.12	1.01	36.10	35.87
Total	99.78	100.89	99.75	93.80	100.27	99.84
Structural formula						
Al	1.845	1.860	1.823	0.096	1.830	1.736
Fe ²⁺	3.038	2.997	3.021	1.038	3.004	3.009
Fe ³⁺	0.079	0.145	0.136	1.734	0.163	0.247
Si	3.038	2.997	3.021	0.038	3.004	3.009
Expt. Phase	aw21 (ski ₁₅) Sp	aw21 (ski ₁₅) Px	aw29 (ski ₁₅) Gt	aw29 (ski ₁₅) Sp	aw29 (ski ₁₅) Px	aw31 (ski ₁₅) Gt
Al ₂ O ₃	2.35	1.71	17.78	2.10	1.65	18.43
FeO _{tot}	89.74	54.41	46.44	88.25	54.04	45.34
SiO ₂	1.85	42.06	35.70	1.93	43.53	35.70
Total	93.94	98.18	99.92	92.28	99.22	99.47
Structural formula						
Al	0.104	0.091	1.756	0.095	0.086	1.823
Fe ²⁺	1.070	2.048	2.991	1.074	2.001	2.996
Fe ³⁺	1.756		0.263	1.757		0.186
Si	0.070	1.893	2.991	0.074	1.928	2.996
Expt. Phase	aw31 (ski ₁₅) Sp	aw37 (ski ₁₅) Gt	aw41 (ski ₁₅) Gt	aw41 (ski ₁₅) Sp	aw48 (ski ₁₅) Gt	aw48 (ski ₁₅) Sp
Al ₂ O ₃	3.76	17.07	16.86	1.78	18.27	5.95
FeO _{tot}	87.86	46.57	47.61	90.09	45.46	87.99
SiO ₂	1.18	35.55	35.60	1.94	35.88	1.23
Total	92.80	99.19	100.07	93.81	99.69	95.17
Structural formula						
Al	0.168	1.701	1.668	0.079	1.805	0.257
Fe ²⁺	1.045	3.006	2.989	1.073	3.008	1.045
Fe ³⁺	1.742	0.287	0.354	1.774	0.179	1.653
Si	0.045	3.006	2.989	0.073	3.008	0.045
Expt. Phase	aw15 (ski ₂₀) Gt	aw15 (ski ₂₀) Px	aw21 (ski ₂₀) Gt	aw21 (ski ₂₀) Sp	aw21 (ski ₂₀) Px	aw26 (ski ₂₀) Gt
Al ₂ O ₃	19.67	5.40	17.53	2.36	1.71	17.87
FeO _{tot}	43.96	50.84	47.07	89.41	54.41	45.76
SiO ₂	35.43	41.22	35.90	1.92	42.06	35.69
Total	99.06	97.46	100.50	93.69	98.18	99.32
Structural formula						
Al	1.945	0.283	1.723	0.105	0.091	1.773
Fe ²⁺	2.972	1.893	2.994	1.072	2.048	3.005
Fe ³⁺	0.112		0.289	1.750		0.217
Si	2.972	1.835	2.994	0.072	1.893	3.005

TABLE 2.—Continued

Expt. Phase	aw26 (ski ₂₀) Px	aw26 (ski ₂₀) Fa	aw29 (ski ₂₀) Gt	aw29 (ski ₂₀) Sp	aw29 (ski ₂₀) Px	aw32 (ski ₃₀) Gt
Al ₂ O ₃	0.97		17.91	2.30	1.44	17.26
FeO _{tot}	53.85	69.54	46.52	88.63	53.90	46.25
SiO ₂	44.41	29.49	35.98	1.96	43.68	35.91
Total	99.23	99.03	100.41	92.89	99.02	99.42
Structural formula						
Al	0.051		1.759	0.103	0.075	1.714
Fe ²⁺	1.991	1.985	2.999	1.075	1.999	3.026
Fe ³⁺			0.244	1.748		0.233
Si	1.964	1.006	2.999	0.075	1.938	3.026
Expt. Phase	aw32 (ski ₂₀) Sp	aw32 (ski ₂₀) Px	aw34 (ski ₂₀) Gt	aw34 (ski ₂₀) Px	aw37 (ski ₂₀) Gt	aw23 (ski ₃₀) Gt
Al ₂ O ₃	2.19	1.49	18.40	3.58	16.04	17.91
FeO _{tot}	87.18	53.51	45.41	52.59	48.49	46.97
SiO ₂	1.86	43.56	35.45	42.09	35.79	36.29
Total	91.23	98.56	99.26	98.26	100.32	101.17
Structural formula						
Al	0.100	0.078	1.824	0.187	1.588	1.747
Fe ²⁺	1.072	1.993	2.892	1.956	3.006	3.003
Fe ³⁺	1.756		0.212		0.400	0.247
Si	0.072	1.940	2.892	1.872	3.006	3.003
Expt. Phase	aw23 (ski ₃₀) Sp	aw23 (ski ₃₀) Px	aw38 (ski ₃₀) Gt	aw38 (ski ₃₀) Sp	u458 (ski ₇₀) Gt	u642 (ski ₃₀) Gt
Al ₂ O ₃	2.34	1.24	16.53	1.36	13.92	14.16
FeO _{tot}	89.34	54.00	47.46	89.36	49.90	50.93
SiO ₂	2.74	43.85	35.56	2.59	34.44	35.46
Total	94.42	99.09	99.58	93.31	98.26	100.55
Structural formula						
Al	0.103	0.065	1.645	0.061	1.418	1.409
Fe ²⁺	1.102	2.003	3.002	1.098	2.976	2.994
Fe ³⁺	1.692		0.351	1.742	0.630	0.602
Si	0.102	1.944	3.002	0.098	2.976	2.994
Expt. Phase	u642 (ski ₃₀) Sp	u541 (ski ₃₀) Gt	u541 (ski ₃₀) Gt	u627 (ski ₃₀) Gt	u532 (ski ₇₀) Gt	u532 (ski ₇₀) Gt
Al ₂ O ₃	0.73	11.40	10.43	9.93	5.54	0.35
FeO _{tot}	89.71	51.93	52.89	54.17	57.75	76.99
SiO ₂	2.79	34.17	34.68	34.41	33.45	17.24
Total	93.23	97.50	98.00	98.51	96.74	94.58
Structural formula						
Al	0.033	1.181	1.078	1.024	0.592	0.015
Fe ²⁺	1.107	3.003	3.042	3.011	3.031	1.630
Fe ³⁺	1.754	0.814	0.838	0.953	1.345	0.724
Si	0.106	3.003	3.042	3.011	3.031	0.630
Expt. Phase	u497 (ski ₈₀) Gt	u532 (ski ₈₀) Gt	u532 (ski ₈₀) Sp	u610 (ski ₈₀) Gt	u610 (ski ₈₀) Sp	u589 (ski ₈₀) Gt
Al ₂ O ₃	4.05	4.58	0.19	4.47	0.13	4.46
FeO _{tot}	60.76	59.49	76.79	59.37	81.19	59.98
SiO ₂	33.21	32.92	12.31	33.06	11.49	33.05
Total	98.02	96.99	92.29	96.80	92.81	97.49
Structural formula						
Al	0.430	0.490	0.008	0.479	0.006	0.475
Fe ²⁺	2.992	2.991	1.466	3.006	1.433	2.989
Fe ³⁺	1.586	1.529	1.060	0.754	1.128	1.547
Si	2.992	2.991	0.466	3.006	0.433	2.989

TABLE 2.—Continued

Expt. Phase	u598 (ski ₉₀) Gt	u524 (sk ₁₀₀) Gt	u524 (sk ₁₀₀) Sp	u548 (sk ₁₀₀) Gt	u548 (sk ₁₀₀) Sp	u548 (sk ₁₀₀) Gt
Al ₂ O ₃	1.94	3.27	0.09			
FeO _{tot}	62.72	61.72	82.70	63.29	83.70	63.85
SiO ₂	32.66	33.46	12.21	32.01	10.48	33.23
Total	97.32	98.45	95.00	95.30	94.25	97.08
Structural formula						
Al	0.209	0.347	0.004			
Fe ²⁺	2.990	3.010	1.450	3.015	1.391	3.069
Fe ³⁺	1.812	1.633	1.097	1.97	1.219	1.862
Si	2.990	3.010	0.450	3.015	0.391	3.069
Expt. Phase	u548 (sk ₁₀₀) Sp	u598 (sk ₁₀₀) Sp	u636 (sk ₁₀₀) Gt	u636 (sk ₁₀₀) Sp	u666 (sk ₁₀₀) Gt	u666 (sk ₁₀₀) Sp
Al ₂ O ₃			0.15			
FeO _{tot}	82.38	81.60	64.84	78.55	64.80	83.81
SiO ₂	11.99	11.55	32.71	17.71	32.67	9.61
Total	94.37	93.15	97.70	96.26	97.47	93.42
Structural formula						
Al			0.016			
Fe ²⁺	1.445	1.434	3.004	1.637	3.006	1.361
Fe ³⁺	1.111	1.132	1.976	0.736	1.980	1.277
Si	0.445	0.434	3.004	0.637	3.006	0.362
Expt. Phase	u693 (sk ₁₀₀) Gt	u693 (sk ₁₀₀) Sp	u702 (sk ₁₀₀) Gt	u636 (fm ₄₀) Gt	u636 (fm ₄₀) Sp	u693 (fm ₄₀) Sp
Al ₂ O ₃	0.94	0.02		0.47		
FeO _{tot}	63.74	85.78	64.71	63.83	75.95	77.13
SiO ₂	33.19	10.44	32.40	32.86	21.41	21.22
Total	97.87	96.24	97.29	97.16	97.36	98.35
Structural formula						
Al	0.101			0.051		
Fe ²⁺	3.031	1.381	2.996	3.029	1.756	1.743
Fe ³⁺	1.837	1.238	2.008	1.891	0.487	0.515
Si	3.031	0.381	2.996	3.029	0.756	0.743
Expt. Phase	aw45req. Gt new	aw45req. Gt old	aw45req. Sp	aw45 req. Px	u642req. Gt new	u642req. Gt old
Al ₂ O ₃	17.89	16.24	1.74	0.99	13.24	9.97
FeO _{tot}	47.02	48.23	89.60	54.61	50.94	54.25
SiO ₂	35.58	35.22	2.60	43.71	34.55	34.85
Total	100.49	99.69	93.94	99.31	98.73	99.07
Structural formula						
Al	1.757	1.617	0.077	0.051	1.346	1.022
Fe ²⁺	2.965	2.975	1.098	2.032	2.980	3.031
Fe ³⁺	0.312	0.432	1.727		0.694	0.915
Si	2.965	2.975	0.098	1.945	2.980	3.031
Expt. Phase	u642req. Sp	u642req. Px	u627req. Gt old	u627req. Sp	u627req. Px	aw69req. Gt rim
Al ₂ O ₃	0.87	0.57	4.48	0.40	0.28	16.55
FeO _{tot}	86.75	54.44	60.65	85.36	54.53	47.99
SiO ₂	4.93	43.51	33.38	8.39	45.38	35.74
Total	92.55	98.52	98.51	94.15	100.19	100.31
Structural formula						
Al	0.039	0.030	0.473	0.018	0.015	1.636
Fe ²⁺	1.188	20.44	2.988	1.314	1.999	2.998
Fe ³⁺	1.584		1.552	1.355		0.369
Si	0.188	1.953	2.988	0.314	1.989	2.998

TABLE 2.—Continued

Expt. Phase	u835req. Gt new	u835req. Gt old
Al ₂ O ₃	12.75	15.50
FeO _{tot}	51.65	49.01
SiO ₂	34.77	35.24
Total	99.17	99.75
Structural formula		
Al	1.293	1.547
Fe ²⁺	2.991	2.983
Fe ³⁺	0.725	0.487
Si	2.991	2.983

0.35–0.45 mm/s, and QS = 0.29–0.75 mm/s; ⁴¹Fe³⁺, IS = 0.04–0.20 mm/s, and QS = 1.05–1.28 mm/s. The hyperfine parameters of our garnet samples indicate that the Fe³⁺ is in octahedral coordination. Although the IS values are a little low compared with the range given in Amthauer et al. (1976), they are significantly larger than those observed for ⁴¹Fe³⁺. Furthermore, our QS values are far too small for tetrahedral occupancy. The FWHM of this doublet is slightly larger than for the Fe²⁺ doublet, ranging mostly between 0.25 and 0.36 mm/s (Table 3). An additional very small peak occurs at ≈1.5 mm/s in the ski₄₀ sample (Fig. 1c). This line position is suggestive of ⁶¹Fe²⁺ and could correspond to a small iron majorite (Fe₂⁺Si₄O₁₂) component in this garnet (Geiger et al., 1991). This peak was not observed in the spectrum from any other sample. At low Fe³⁺ contents, the Fe³⁺ doublet forms an ill-defined shoulder on the low-velocity Fe²⁺ peak (Fig. 1a). As a result, the Fe³⁺ line positions and calculated Fe³⁺/Fe_{tot} are subject to relatively larger uncertainties compared with the samples richer in skiaigite component. The Fe³⁺/Fe_{tot} ratios calculated from the relative areas of the room-temperature spectra, assuming equal recoil-free fractions for Fe²⁺ and Fe³⁺ on the two sites, are in broad agreement with those calculated from the microprobe-determined compositions (Table 3). However, the Mössbauer Fe³⁺/Fe_{tot} values systematically tend to overestimate the true value by about 15% (relative), which is probably because of our assumption of equal recoil-free fractions for Fe²⁺ and Fe³⁺. The differences cannot be entirely reconciled by considering the uncertainties of the Mössbauer and microprobe methods, both of which are on the order of ≈0.01. The details of the Mössbauer results will be reported elsewhere.

Cell edges and molar volumes

Almandine-skiagite solutions. The garnet cell edges, a_0 , are listed in Table 1 and shown in Figure 2. They increase linearly with increasing skiaigite content. A weighted least-squares fit to the data gives $a_0 = 11.5244(4) +$

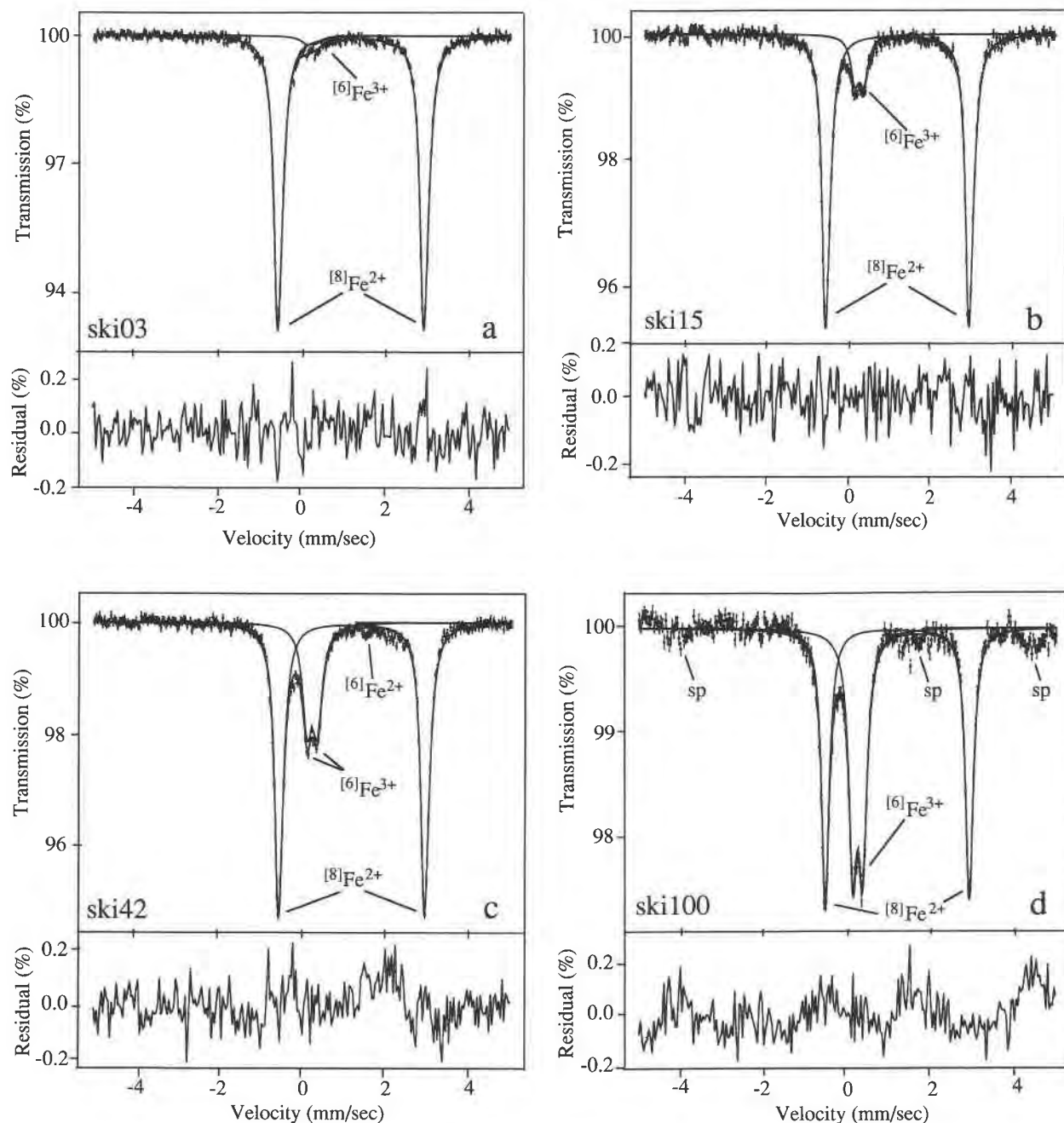


Fig. 1. Room-temperature Mössbauer spectra of four garnet samples: (a) ski₀₃, (b) ski₁₅, (c) ski₄₂, and (d) ski₁₀₀. The doublet with a large quadrupole splitting (QS) corresponds to Fe²⁺ in dodecahedral coordination. The doublet with a very small QS that grows with increasing skiagite content is assigned to Fe³⁺ in octahedral coordination (see text).

$0.2034(6)X_{\text{ski}}$, with $\chi^2 = 1.40$. Higher order terms did not result in any significant improvement in the fit. The lattice parameters were weighted according to the standard deviations given in Table 1, and the compositions were weighted assuming estimated standard errors (of the mean) of ± 0.01 for $X_{\text{ski}} < 0.96$ and ± 0.005 for $X_{\text{ski}} > 0.96$, based upon the microprobe analyses. End-member skiagite has a cell edge of $a_0 = 11.7278(6)$ Å. Likewise, a cell

edge of $a_0 = 11.5244(4)$ Å is obtained for pure almandine. This value is ~ 0.004 Å smaller than the values of the almandine samples synthesized in this study; however, our almandine samples contain a small amount of Fe³⁺ (Table 3).

Skiagite. End-member skiagite was successfully synthesized from both slag and oxide mixtures. Unfortunately, variable amounts of spinel and stishovite were

TABLE 3. Hyperfine parameters and $\text{Fe}^{3+}/\text{Fe}_{\text{tot}}$ ratios for almandine-skiagite garnet

Sample	Fe^{2+}		FWHM (mm/s)	Fe^{3+}		FWHM (mm/s)	χ^2	$\text{Fe}^{3+}/\text{Fe}_{\text{tot}}$ area ratio
	QS*	IS*		QS*	IS*			
aw18(ski ₀₂)	3.52	1.29	0.25	0.25	0.32	0.46	1.52	0.045
aw14(ski ₀₃)	3.51	1.30	0.25	0.22	0.31	0.36	1.19	0.030
aw45(ski ₀₇)	3.54	1.30	0.24	0.18	0.34	0.34	1.42	0.072
aw25(ski ₀₈)	3.51	1.30	0.25	0.21	0.33	0.29	1.41	0.074
aw26(ski ₀₈)	3.54	1.30	0.27	0.21	0.34	0.32	1.54	0.061
aw30(ski ₀₉)	3.53	1.30	0.25	0.22	0.35	0.30	1.13	0.077
aw37(ski ₁₅)	3.52	1.30	0.25	0.21	0.34	0.29	1.05	0.141
aw37(ski ₂₁)	3.51	1.30	0.25	0.23	0.35	0.25	1.17	0.156
aw47(ski ₃₀)	3.50	1.30	0.24	0.23	0.33	0.29	1.99	0.218
uhp458(ski ₃₁)	3.51	1.29	0.28	0.23	0.35	0.28	2.04	0.191
uhp541(ski ₄₂)	3.52	1.30	0.25	0.25	0.34	0.28	1.34	0.271
uhp627(ski ₅₀)	3.48	1.30	0.29	0.24	0.35	0.30	1.25	0.299
uhp497(ski ₇₉)	3.47	1.29	0.23	0.25	0.35	0.24	1.26	0.404
uhp598(ski ₉₀)	3.50	1.30	0.24	0.24	0.36	0.25	1.24	0.429
uhp636(ski ₁₀₀)	3.46	1.31	0.23	0.24	0.35	0.26	2.11	0.459
uhp702(ski ₁₀₀)	3.46	1.31	0.23	0.24	0.36	0.25	1.88	0.462

Note: measurements made at 298 K and 1 atm.

* Millimeters per second measured relative to α Fe metal at 298 K. Uncertainties are about ± 0.01 mm/s for both QS and IS and ± 0.01 for $\text{Fe}^{3+}/\text{Fe}_{\text{tot}}$. The area ratio assumes the same recoil-free fraction for Fe^{2+} and Fe^{3+} on the different sites.

also present in the products. The best yield of garnet (on the order of 60–70%) was obtained from stoichiometric mixtures of ferrosilite + hematite. The minimum pressure at which the end-member skiagite is stable is about 9.3 GPa, based upon the observed growth of garnet on garnet seeds in backscattered electron images from experiment uhp666.

The molar volume (V_{298}) for the skiagite end-member is 121.44 cm³. Karpinskaya et al. (1982) were the first to report the synthesis of skiagite. They produced a mixture of garnet, spinel, and stishovite? at 800 °C and 10.0 GPa and reported a molar volume of 120.9 ± 1.5 cm³ for the garnet. The large uncertainty in their measurement is attributable to their analytical method (Gandolfi camera) and the presence of spinel, which has many overlapping reflections with the garnet. The molar volume of skiagite determined in this study is in good agreement with that predicted from crystal structure considerations by Novak and Gibbs (1971), 121.2 cm³.

Almandine. The molar volume of pure $\text{Fe}_3^{2+}\text{Al}_2\text{Si}_3\text{O}_{12}$ determined from extrapolation of our binary garnet data, 115.23 ± 0.01 cm³, falls within the range of values reported in the literature: 115.28 cm³ from Cressey et al. (1978) and Geiger et al. (1987), 115.20–115.34 cm³ from Bohlen et al. (1983b), 115.25–115.43 cm³ from Hsu (1968), and 115.19–115.40 cm³ from Keesman et al. (1971). Our garnet sample with the smallest molar volume, 115.34 cm³, was synthesized in the presence of excess SiO_2 and Fe metal, yet it contained detectable Fe^{3+} (aw1, aw6; Table 1). This confirms that small quantities of Fe^{3+} are readily accommodated in almandine at very low f_{O_2} , even in the presence of Fe metal. The coexistence of Fe^{3+} -bearing almandine and Fe metal suggests that macroscopically stoichiometric almandine may not be stable, at least at the conditions of the syntheses.

The range in molar volumes cited above, although small, is significantly greater than the accuracy and precision of the measurement of the unit-cell edge by X-ray

diffraction. This points to small differences in composition, possibly even involving defects, among the various synthesized almandine samples. Some of the almandine samples reported by Hsu (1968) were synthesized hydrothermally and could well contain H_4O_4 groups that would increase the garnet unit-cell edge (e.g., Meagher, 1980). Our results document that the incorporation of a skiagite component also increases the unit-cell edge. With the experimental difficulty in maintaining all Fe in the Fe^{2+} state, many of the reported values larger than our extrapolated value probably reflect the presence of variable amounts of Fe^{3+} . This has sometimes led to the assump-

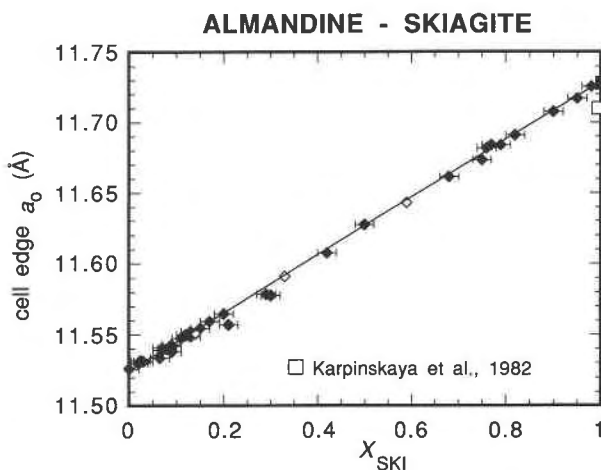


Fig. 2. Cell edge, a_0 , vs. composition for almandine-skiagite solutions. The linear regression shown is based upon the solid data points only. The solid diamonds are data from this study. The solid square at the skiagite end-member is in perfect agreement with the extrapolated value from this regression. The open diamonds indicate the garnet composition attending reequilibration at lower pressure. The open square is from Karpinskaya et al. (1982), which is the only other report of a synthesis of skiagite.

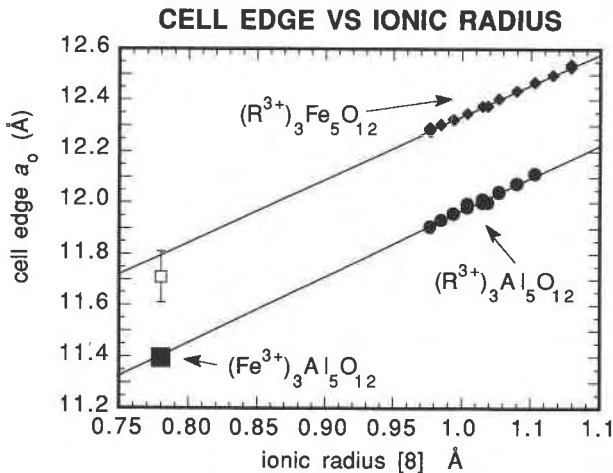


Fig. 3. Unit-cell edge vs. the dodecahedral cation ionic radius for rare-earth garnets with $R_3^{3+}Fe_5O_{12}$ and $R_3^{3+}Al_5O_{12}$ stoichiometry. The ionic radii are from Shannon (1976). The cell edge data are from Rubinstein and Barns (1964), JCPDS X-ray diffraction cards 22-1093, 32-12, 32-16, and the compilations of Hawthorne (1981) and Stadnik (1984). The open square is for the end-member Fe_8O_{12} (garnet), based on extrapolation from $(Y,Fe^{3+})_3Fe_5^{3+}O_{12}$ garnet solution, with the error bar assuming an uncertainty in composition of $\pm 10\%$ (relative) (Paladino and Maguire, 1970). The solid square shows the position of the hypothetical $Fe_3^{3+}Al_5O_{12}$ (garnet) obtained by extrapolation.

tion that the lower the unit-cell edge, the lower the Fe^{3+} content, and therefore the closer to the ideal stoichiometric almandine. However, Bohlen et al. (1983b) synthesized almandine garnet with cell edges of 11.520 and 11.521 Å, considerably smaller than our extrapolated value. Minor substitution of another type of component would appear to be a likely explanation. One such possibility is an Fe^{3+} -bearing component analogous to YAG, $Fe_3^{3+}Al_5O_{12}$. In almandine, this would be achieved through the coupled substitution of Fe^{3+} for Fe^{2+} and Al for Si on the dodecahedral and tetrahedral sites, respectively. Yoder and Keith (1951) demonstrated a complete solid solution between $Mn_3Al_2Si_3O_{12}$ and $Y_3Al_5O_{12}$, suggesting that there is no difficulty in substituting Al for Si on the tetrahedral sites of silicate garnets. A small amount of ^{18}O may be inferred to occur in $Y_3Fe_5O_{12}$ garnet in equilibrium with Fe_2O_3 at high temperatures (Paladino and Maguire, 1970). At 1450 °C and 1 atm, Paladino and Maguire (1970) showed an excess of Fe_2O_3 in the garnet, equivalent to 0.9 mol% Fe_8O_{12} , which caused a decrease in a_0 of 0.006 Å. In Figure 3, we have plotted the unit-cell edge vs. dodecahedral cation ionic radius for rare-earth $R_3^{3+}Al_5O_{12}$ and $R_3^{3+}Fe_5O_{12}$ garnets. Both the ferrite garnet and aluminate garnet define linear relationships with nearly identical slopes, emphasizing the strong influence the dodecahedral cation plays in determining the molar volume of these garnets. A linear extrapolation to 0.78 Å (Fe^{3+} in eightfold coordination) yields $a_0 = 11.39$ Å, or $V = 111.0$ cm³, for the hypothetical $Fe_3^{3+}Al_5O_{12}$ component. The unit-cell edge reported by Bohlen et al. (1983b) would correspond to about 2 mol% of this com-

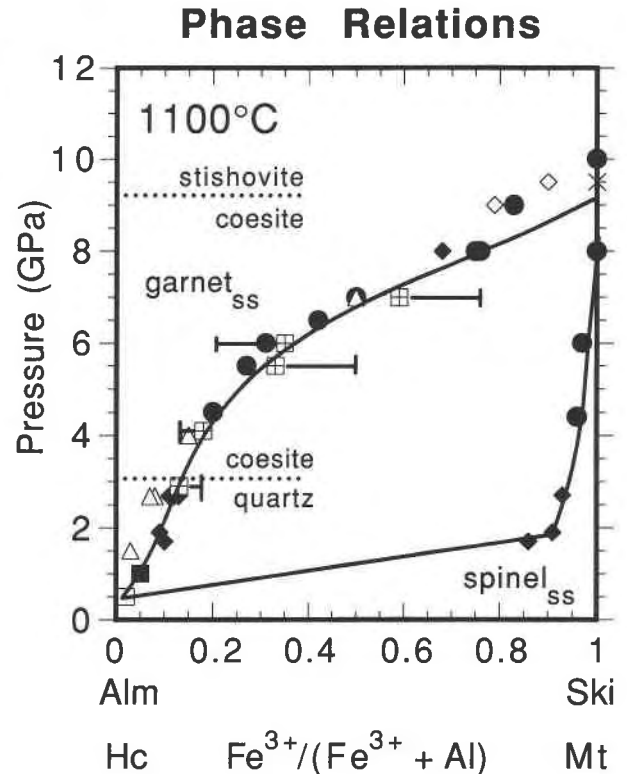


Fig. 4. Phase relations for almandine-skiagite solutions as a function of pressure up to 12.0 GPa at 1100 °C. The coexisting spinel composition, defining part of the loop, is shown projected through Fe_2SiO_4 , which makes the loop pseudodivariant. The positions of the SiO_2 polymorph transitions are also shown for reference. Open triangles are garnet $\pm SiO_2$; open diamonds are garnet + hematite + SiO_2 ; closed diamonds are garnet + spinel + SiO_2 + pyroxene; closed circles are garnet + spinel + SiO_2 ; crossed squares are the reequilibration experiments with the approach to equilibrium shown; the \times indicates no reaction; the closed square is garnet + fayalite + spinel + quartz; the open square is the terminal reaction almandine = hercynite + fayalite + quartz, calculated from the thermodynamic data base of Holland and Powell (1990).

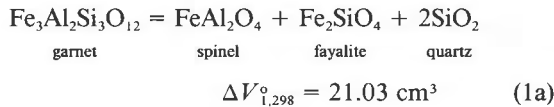
ponent, consistent with the Fe^{3+}/Fe_{tot} of 0.02 ± 0.01 measured by Mössbauer spectroscopy of their sample. This substitution would be favored by an SiO_2 -poor composition and high Al_2O_3 activity. It is therefore possible that minor amounts of solid solution can act to reduce the unit-cell edge of almandine as well as increase it, and the assumption that the lowest cell edge corresponds to the most stoichiometric composition is not necessarily valid. The unit-cell edge from the regression of our data should provide the best estimate for pure stoichiometric almandine.

Phase relations

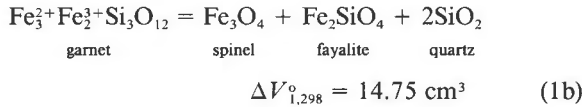
The extent of Fe^{3+} substitution for Al in garnet increases strongly with increasing pressure (Table 1). The results can be conveniently viewed in terms of an isothermal quasi-divariant system projected from a point along the Fe_2SiO_4 - SiO_2 join onto the Al- Fe^{3+} pressure plane. This

is illustrated in Figure 4, which shows the phase relations with the garnet solutions as a function of pressure. For example, at 1100 °C, the skiaigite component saturates at 13, 43, and 75 mol% at 2.7, 6.5, and 8.0 GPa, respectively. The skiaigite end-member is stable above ≈ 9.3 GPa. When the starting material has an $\text{Fe}^{3+}/\text{Fe}_{\text{tot}}$ content that differs from the stable garnet composition at a particular pressure, a multiphase assemblage appears. The coexisting phases and their compositions obviously depend on the starting bulk composition. However, here we are concerned with compositions that lie on or very close to the almandine-skiagite join.

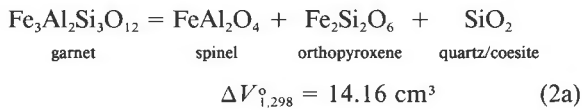
Under dry conditions and low pressures, the stability field of garnet terminates with the equilibrium



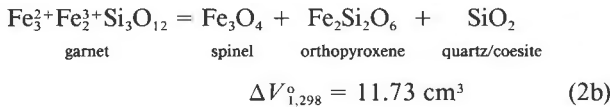
or



(Keesman et al., 1971; Hensen, 1970). Molar volumes are from this study and Holland and Powell (1990). Reaction 1a, the essentially Fe^{3+} -free reaction, lies at about 0.5 GPa at 1100 °C (Hensen, 1970). At higher pressure, fayalite + quartz becomes unstable relative to orthopyroxene, and the garnet composition is governed by the equilibrium



or



The $\Delta V_{1,298}^{\circ}$ given is with coesite. This phase assemblage is shown at a representative pressure of 2.7 GPa in Figure 5, plotted in the composition space $\text{FeO}-\text{SiO}_2-(\text{AlO}_{1.5} + \text{FeO}_{1.5})$. The coexisting orthopyroxene contains only minor amounts of Al, ≤ 0.09 cations on a six O atom basis for all experiments. The coexisting spinel is an Fe_3O_4 - Fe_2SiO_4 - FeAl_2O_4 solution in which the FeAl_2O_4 component decreases sharply with increasing pressure (Table 1, Fig. 4). For example, the spinel in equilibrium with garnet (ski_{13}) at 2.7 GPa has a composition of 87% Fe_3O_4 + 8% Fe_2SiO_4 + 5% FeAl_2O_4 . With increasing pressure there is a progressive increase in the solubility of Fe_2SiO_4 in the spinel, such that orthopyroxene + Si-poor spinel becomes unstable relative to Si-rich spinel + SiO_2 . This results in the following high-pressure equilibrium with garnet (Fig. 5):

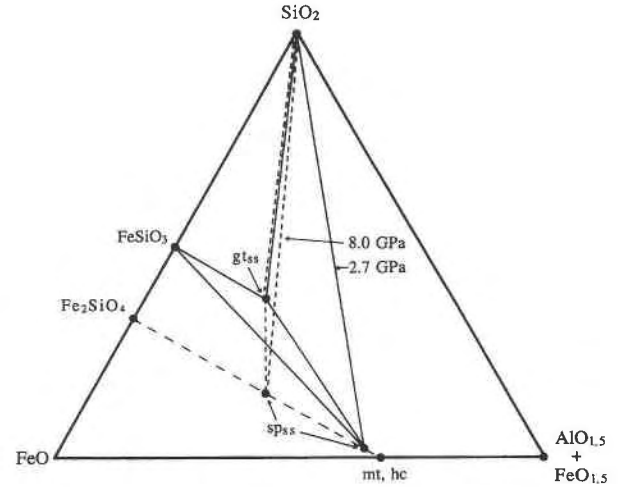
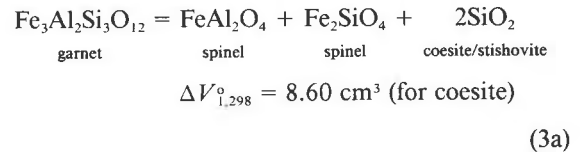
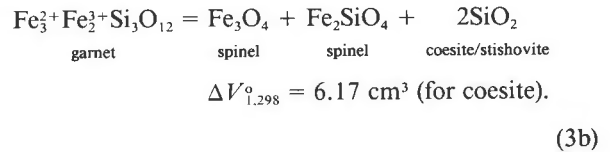


Fig. 5. Plot of the system $\text{FeO}-\text{SiO}_2-(\text{AlO}_{1.5} + \text{FeO}_{1.5})$ showing representative phase assemblages at 2.7 and 8.0 GPa and 1100 °C. Note the shift in spinel composition with increasing pressure.



or



The $\Delta V_{1,298}^{\circ}$ of γ Fe_2SiO_4 (spinel), 41.77 cm^3 , is extrapolated from the Al-free spinels in Table 1 and from Canil and O'Neill (unpublished data). At high pressure, the spinel contains even less Al. For example, the spinel in equilibrium with garnet (ski_{82}) is essentially 55% Fe_3O_4 + 45% Fe_2SiO_4 with < 1.0 mol% FeAl_2O_4 (Table 1). Note that the spinel compositions in Figure 4 have been projected through Fe_2SiO_4 to plot them on the diagram. Thus, the loop shown is quasi-divariant and could cause the false impression that the spinel coexisting with skiaigite-rich garnets is virtually pure magnetite, when in fact they contain appreciable Fe_2SiO_4 . The increase in Fe_2SiO_4 content of the spinel with increasing pressure is evident when comparing the compositions of the spinels in the phase assemblages at 2.7 and 8.0 GPa in the projection of Figure 5.

In several experiments, the starting $\text{Fe}^{3+}/\text{Fe}_{\text{tot}}$ clearly deviated from the stable garnet composition, causing phases other than those involved in Reactions 2 and 3 to appear. When the starting composition was too oxidized (excess Fe^{3+}), such as in experiment uhp497, hematite appeared instead of spinel (Table 1). When the starting composition was too reduced (excess Fe^{2+}), an SiO_2 deficient assemblage was produced. At high pressure, py-

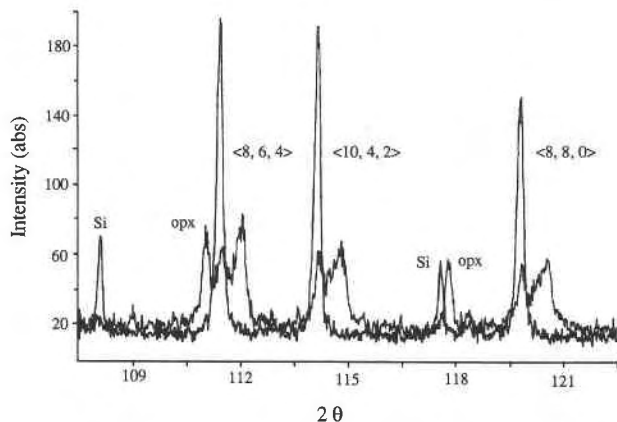


Fig. 6. High-angle $\langle 8, 6, 4 \rangle$, $\langle 10, 4, 2 \rangle$, and $\langle 8, 8, 0 \rangle$ reflections from a reequilibrated garnet (short peaks) and its ski_{78} precursor (monochromated $\text{CoK}\alpha_1$ radiation).

roxene appeared at the expense of coesite [uhp532 (ski_{70})]. It was identified as clinoferrosilite, on the basis of several low-intensity peaks on the X-ray diffraction pattern. The occurrence of clinoferrosilite rather than orthoferrosilite at 8.0 GPa and 1100 °C is consistent with the results of Akimoto et al. (1965). In a lower pressure experiment, aw26, fayalite was produced at the expense of quartz.

Reversals. Three experiments were performed where a previously synthesized garnet was reequilibrated at lower pressure. A new garnet, richer in almandine content, formed (Figs. 2, 4, 6). In these experiments, therefore, equilibrium was approached from the direction of relatively high Fe^{3+} in the garnet. Two distinct peaks at high 2θ are observable in the powder diffractograms from these experiments, an example of which is presented in Figure 6. One peak corresponds to the original garnet, which has not fully reacted, and the other peak corresponds to the newly crystallized garnet. Only the cell edge of the new garnet is reported in Table 1. The presence of two distinct peaks rather than a single broad peak shows that the new garnet formed by the breakdown of the original garnet followed by nucleation and growth rather than by coupled diffusion of Al and Fe^{3+} . This is confirmed by the textures observed in backscattered electron images.

The approach to equilibrium from the direction of relatively high Al content in the garnet was tested in two experiments (aw69, uhp835; see Table 1). In aw69, a previously synthesized assemblage of garnet (ski_{13}) + spinel + pyroxene + quartz was reacted at a higher pressure of 4.1 GPa. The resulting large garnets ($> 10 \mu\text{m}$) were zoned, and small grains (3–8 μm) showed a range in composition. The most skiaigite-rich composition (ski_{18}) was taken as that most closely representing the maximum skiaigite solubility at the higher pressure, and it is given in Tables 1 and 2. In the other experiment (uhp835) a mixture of ferrosilite, hematite, and a previously synthesized garnet (ski_{21}) were reacted at 6.0 GPa. Skiaigite-rich rims were observed to have grown on the original garnet grains. The rim compositions were variable, presumably because of

a heterogeneous distribution of hematite at the required fine scale in the starting mixture. The most skiaigite-rich rim was taken to be closest to the equilibrium composition (Tables 1, 2). The difficulty in obtaining homogeneous garnet in these experiments is analogous to the difficulty in synthesizing garnet solid solutions from oxide mixes, as described earlier. In contrast, the garnets produced from glass or slag were not zoned. The lack of zoning under P - T conditions where nonequilibrium garnets show zoning suggests that the use of glasses or slags produced equilibrium garnet compositions.

Skiaigite solubility in almandine has a strong positive pressure dependence (Fig. 4). A sharp increase in skiaigite solubility occurs at pressures above ≈ 5.0 GPa. The change in slope illustrated in Figure 4 is attributable to the disappearance of pyroxene as a coexisting phase and represents the transition from breakdown Reactions 3 to 4. The strong pressure dependence in skiaigite solubility can be understood in part by considering the $\Delta V_{1,298}^\circ$ for the skiaigite breakdown Reaction 3b. With coesite as the SiO_2 polymorph, $\Delta V_{1,298}^\circ = +6.17 \text{ cm}^3$. Therefore, skiaigite is expected to be favored with increasing pressure. Such an argument does not hold in the stishovite stability field, however, where Reaction 3b gives $\Delta V_{1,298}^\circ = -7.5 \text{ cm}^3$. Skiaigite should be destabilized by the transformation from coesite to stishovite. This is consistent with the absence of garnet in a reconnaissance experiment using a stoichiometric mixture of ferrosilite and hematite performed at 13.0 GPa and 1100 °C. It appears that at 1100 °C, end-member skiaigite is only stable within a narrow pressure range just above the coesite-stishovite transition.

The Al content of the coexisting spinel varies widely depending on the amount of skiaigite in the garnet. At low pressures, nearly pure hercynite coexists with almandine (Reaction 1a, 1b; Fig. 4). The incorporation of a small skiaigite component in the garnet drives the spinel to magnetite-rich compositions (Fig. 4). Except at dilute skiaigite compositions ($< 10 \text{ mol}\%$ skiaigite), hercynite is only a minor component in the spinel. This indicates that Al is strongly partitioned into garnet.

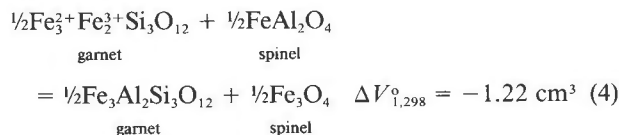
An iron majorite component?

Majorite, $(\text{Mg}, \text{Fe}^{2+})_4\text{Si}_4\text{O}_{12}$, is believed to be an abundant garnet component at depths > 350 km (Ringwood, 1975). According to Akaogi and Akimoto (1977), the solubility of iron majorite in almandine reaches a maximum of 40 mol% between 9.0 and 10.0 GPa at 1000 °C. They estimated a unit-cell edge of 11.595 Å for the $\text{Fe}_4^{2+}\text{Si}_4\text{O}_{12}$ end-member, based on extrapolation. However, the solubility of an iron majorite component in Fe^{3+} -bearing garnet has not been previously studied. No significant excess of Si (> 3.0 cations pfu) was detected by the electron microprobe. A trace of $^{60}\text{Fe}^{2+}$ was detected in only one Mössbauer spectrum, sample uhp541, with a composition of 40% skiaigite + 60% almandine (Fig. 1c). This suggests that at least small amounts of iron majorite can be accommodated in the presence of Fe^{3+} . Confident identification of $^{60}\text{Fe}^{2+}$ in the end-member samples is

hampered by the presence of small amounts of spinel, which have overlapping peak positions with any $^{61}\text{Fe}^{2+}$ in the garnet (compare Fig. 1c and 1d). Two experiments were performed in the $\text{FeO-FeO}_{1.5}\text{-SiO}_2$ subsystem with a bulk composition of 60% skiaigite and 40% iron majorite to test for the possible solubility of iron majorite in skiaigite [uhp636 ($\text{ski}_{60}\text{-fm}_{40}$) and uhp693 ($\text{ski}_{60}\text{-fm}_{40}$)]. Garnets with cell edges slightly smaller than that for the pure skiaigite end-member were produced in both experiments (Table 1). However, a small amount of Al was detected in the garnets by microprobe, indicating some contamination had occurred, probably during loading of the capsule. The smaller cell edges are in good agreement with the determined almandine content in these samples. These experiments suggest that the solubility of iron majorite in skiaigite is very small; otherwise the measured cell edges would have deviated significantly from the pure end-member value. The garnet in equilibrium with these Fe_2SiO_4 -rich spinels + SiO_2 should have the greatest possible majorite content, yet little if any is indicated. However, that does not preclude significant solubility of Fe^{3+} in majorite-rich garnet at higher pressures. In fact, a recent synthesis of $(\text{Mg}_{0.8}\text{Fe}_{0.2})\text{SiO}_3$ garnet at 1800 °C and 18 GPa was found to have up to 14% of its Fe in the ferric state, corresponding to 5 mol% of an $\text{Fe}_2^{3+}\text{Fe}_2^{2+}\text{-Si}_3\text{O}_{12}$, or skiaigite, component (O'Neill et al., 1993).

Free energy of formation of $\text{Fe}_2^{3+}\text{Fe}_2^{2+}\text{Si}_3\text{O}_{12}$ at 1100 °C

An estimate of $\Delta_f G_{1,1373}^\circ$ for skiaigite can be made from the experiments in Table 1 by considering the exchange reaction



for which

$$\begin{aligned} \Delta G_{P,1373}^\circ &= -\frac{1}{2}RT \ln \frac{a_{\text{Fe}_3\text{O}_4}^{\text{sp}} a_{\text{Fe}_2^{3+}\text{Fe}_2^{2+}\text{Si}_3\text{O}_{12}}^{\text{gl}}}{a_{\text{FeAl}_2\text{O}_4}^{\text{sp}} a_{\text{Fe}_2^{3+}\text{Fe}_2^{2+}\text{Si}_3\text{O}_{12}}^{\text{gl}}} \\ &= -RT \ln K_d - RT \ln K_\gamma \end{aligned}$$

where $a = (X\gamma)^2$ for both spinel and garnet. The standard state is the pure substance at 1 bar and the temperature of interest. Figure 7 is a plot of $\ln K_d$ as a function of pressure. With $\int_1^P \Delta V_{P,T} dP = \Delta V_{1,298}^\circ \Delta P$ and both the garnet and spinel as ideal solid solutions, $\ln K_d$ should be a linear function of pressure with slope $d(\ln K_d)/dP = d(\ln K)/dP = -\Delta V_{1,298}^\circ/RT$. A line with this slope ($1.069 \times 10^{-5}/\text{bar}$) is drawn in Figure 7, with the actual position fitted by eye. The lack of agreement with the data indicates that one or both of the phases are nonideal. Nonideality in the ternary $\text{Fe}_3\text{O}_4\text{-FeAl}_2\text{O}_4\text{-Fe}_2\text{SiO}_4$ spinels is plausible. However, nothing is presently known about the thermodynamic mixing properties of 2-3 spinels, such as Fe_3O_4 and FeAl_2O_4 , with 4-2 silicate spinels (O'Neill and Navrotsky, 1984). Restricting our analysis to those data

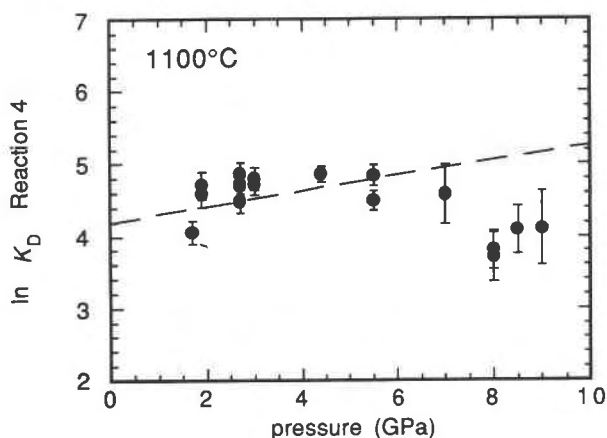


Fig. 7. Plot of $\ln K_d$ vs. pressure for Reaction 4. The uncertainties are 1σ , computed from the microprobe analyses of the garnet and spinel. The slope of the line shown was constrained by $d(\ln K)/dP = -\Delta V_{1,298}^\circ/RT$; however, the actual position is from a best fit by eye. The slope of $1.069 \times 10^{-5}/\text{bar}$ assumes ideal mixing behavior (i.e., $K = K_d$).

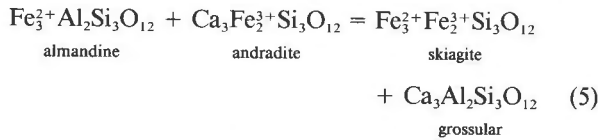
below 4.5 GPa, where $X_{\text{Fe}_2\text{SiO}_4}$ are sufficiently small, we can reasonably project our spinel compositions from Fe_2SiO_4 onto the $\text{Fe}_3\text{O}_4\text{-FeAl}_2\text{O}_4$ binary and calculate $\gamma_{\text{FeAl}_2\text{O}_4}$ and $\gamma_{\text{Fe}_3\text{O}_4}$, following the model of O'Neill and Navrotsky (1984). If we assume ideal mixing in the coexisting garnet, the $\gamma_{\text{ski}}/\gamma_{\text{alm}}$ term will drop out of the equation. Alternatively, Luth et al. (1990) provide an estimate for the Al- Fe^{3+} mixing properties in garnets of $W_{\text{Al-Fe}^{3+}} = 3.7$ kJ/mol on a per cation basis. Treating the spinel solid solutions in the above manner and assuming $\int_1^P \Delta V_{P,T} dP = \Delta V_{1,298}^\circ \Delta P$ we can express $\Delta G_{1,1373}^\circ$ for the exchange Reaction 4 as:

$$\begin{aligned} \Delta G_{1,1373}^\circ &= -RT \ln K_d - RT \ln \frac{\gamma_{\text{Fe}_3\text{O}_4}}{\gamma_{\text{FeAl}_2\text{O}_4}} \\ &\quad - P\Delta V_{1,298}^\circ \text{ (Reaction 4)} + RT \ln \frac{\gamma_{\text{ski}}}{\gamma_{\text{alm}}} \end{aligned}$$

From the ten data below 4.5 GPa, we obtain $\Delta G_{1,1373}^\circ = -34.63$ kJ/mol, with a σ of 1.51 kJ if mixing in the garnet is ideal, and $\Delta G_{1,1373}^\circ = -31.83 \pm 1.57$ kJ/mol if the interaction parameter of Luth et al. (1990) is considered. Taking the free energies of formation for almandine, magnetite, and hercynite at 1373 K derived from Holland and Powell (1990) and using entropies of Si and O_2 from Robie et al. (1978) and of Fe from Holmes et al. (1986) gives for skiaigite $\Delta_f G_{1,1373}^\circ$ (ski) = -2975.2 ± 3.0 kJ/mol for the case of ideal almandine-skiaigite mixing and $\Delta_f G_{1,1373}^\circ$ (ski) = -2980.8 ± 3.1 kJ/mol with the symmetric interaction parameter, $W_{\text{Al-Fe}^{3+}}$, of Luth et al. (1990). The data of Holmes et al. (1986) were used for Fe because Holland and Powell (1990) only tabulate data for α Fe, and our calculations, at 1373 K, are in the γ Fe field. The quoted uncertainties do not include any con-

tribution derived from uncertainties in the thermodynamic data for the other phases.

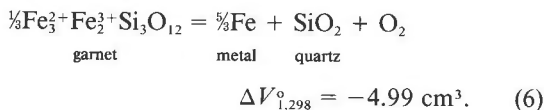
With the above result and Holland and Powell's data for grossular, almandine, and andradite combined, the ΔG for the reciprocal reaction,



is estimated to be $\Delta G_{P,1373}^{\circ}(\text{kJ/mol}) = 40.2 - 0.7P$ (GPa) from Reaction 5 with ideal mixing, and $\Delta G_{P,1373}^{\circ}(\text{kJ/mol}) = 32.8 - 0.7P$ using the interaction parameter of Luth et al. for Al-Fe³⁺ mixing. The relatively large value of $\Delta G_{P,1373}^{\circ}$ (Reaction 5) is presumably due to the fact that the octahedral cation to O bond distances in garnet (i.e., Al-O and Fe³⁺-O) are a strong function of the dodecahedral cation size and vice versa: the ¹⁸Ca-O and Fe²⁺-O bond distances depend on the size of the octahedral cation. If that is true, then the analogous reciprocal reaction involving the magnesium garnets, pyrope and khoharite (Mg₃Fe₂³⁺Si₃O₁₂), would be expected to have a similar ΔG as the Fe-bearing Reaction 5 because of the similarity in ionic radii of Mg and Fe²⁺ in dodecahedral coordination (Shannon, 1976).

The value of ΔG for the reciprocal Reaction 5 is intermediate between the two values, 25 and 50 kJ/mol, assumed by Luth et al. (1990). When applied to their equilibria used to calculate mantle f_{O_2} , resulting f_{O_2} values generally fall within the range of FMQ ± 1.5 log units (Luth et al., 1990, their Fig. 7a-7c). This implies redox conditions in the garnet lherzolite facies of the upper mantle similar to those observed in the spinel lherzolite facies (Wood et al., 1990).

The question of whether pure almandine is stable in light of our experiments with excess Fe metal and quartz can be assessed by considering the reaction



If the Fe and quartz are pure ($a = 1.0$), $\log K_6 = \log f_{\text{O}_2} - \frac{1}{2}\log a_{\text{ski}}$. With data for β quartz from Holland and Powell (1990) for O₂ and Fe from Robie et al. (1978) and Holmes et al. (1986), $\log K_6 = -12.06$ at 1373 K and 2.0 GPa, assuming ideal mixing in the garnet. With a $\log f_{\text{O}_2}$ defined by the O₂ buffer assemblage quartz + fayalite + Fe (QFI), extrapolated to 1373 K and 2.0 GPa ($\log f_{\text{O}_2} = -13.29$; O'Neill, 1987), this yields $\log a_{\text{ski}} = -3.69$ or $X_{\text{ski}} = 1.4$ mol%. The QFI buffer lies close to the low f_{O_2} stability limit for almandine (Woodland and Wood, 1989), and, therefore, the skiaigite content under these conditions should be near the minimum possible. The calculated skiaigite content is in close agreement with that indicated from the unit-cell edge measurements of our experiments with excess Fe and SiO₂ performed at higher temperature ($X_{\text{ski}} = 2$ mol% in aw1, aw6; Table 1). The

sign of $\Delta V_{1,298}^{\circ}$ (Reaction 6) shows that slightly lesser skiaigite contents would be favored at lower pressure. The influence of temperature is not known.

CONCLUSIONS

Fe³⁺ is readily accommodated in the aluminous garnet almandine. Substitution of Fe³⁺ for Al on the octahedral sites can be considered in terms of an Fe₂³⁺Fe₁²⁺Si₃O₁₂ (skiaigite) component. The maximum extent of skiaigite solubility in almandine is strongly pressure dependent, increasing with increasing pressure. At high pressure, the solid solution is complete. End-member skiaigite is stable at pressures above ≈ 9.3 GPa. The molar volume of skiaigite, 121.45 ± 0.01 cm³, agrees with the value reported by Karpinskaya et al. (1982), although our value is both more accurate and more precise. Molar volumes of the almandine-skiaigite solid solutions vary linearly with composition. The molar volume of almandine retrieved from the fit to our data is 115.23 ± 0.01 cm³. Small differences from this value reported by other workers may be due to minor amounts of other components.

The maximum solubility of Fe³⁺, or the skiaigite component, in garnet at a given pressure is controlled through the equilibrium between garnet and the assemblage spinel + SiO₂ + orthopyroxene at low pressures (<5.0 GPa) or spinel + SiO₂ at high pressure. The coexisting spinel becomes progressively richer in Fe₂SiO₄, with increasing pressure to the point where the Fe³⁺/Fe_{tot} of the spinel approaches that of the garnet. The very low Al content of both the coexisting spinel and pyroxene indicates that Al is strongly partitioned into garnet.

End-member skiaigite probably becomes unstable with increasing pressure in the stishovite stability field. As a result, this garnet is only stable within a rather narrow pressure range, at least at 1100 °C. Iron majorite substitution in skiaigite is negligible at the pressures of this study. The demonstrated ability of a pyralspite garnet sample to contain substantial Fe³⁺ suggests that garnet could be the dominant Fe³⁺-bearing phase in the mantle at pressures above the stability limit of aluminate-chromite spinel.

ACKNOWLEDGMENTS

This project was made possible in part by a fellowship to A.B.W. from the Alexander von Humboldt Stiftung. Its support is gratefully acknowledged. D. Canil, V. von Seckendorf, C. McCammon, and F. Seifert are thanked for their helpful advice and discussion during the course of the project. The manuscript was improved through the thoughtful reviews of C. Manning, W. Dollase, D. Perkins, and an anonymous reviewer.

REFERENCES CITED

- Akaogi, M., and Akimoto, S. (1977) Pyroxene-garnet solid solution equilibria in the systems Mg₂Si₂O₇-Mg₃Al₂Si₂O₁₂ and Fe₂Si₂O₇-Fe₃Al₂Si₂O₁₂ at high pressures and temperatures. *Physics of the Earth and Planetary Interiors*, 15, 90-106.
- Akimoto, S., Katsura, T., Syono, Y., Fujisawa, H., and Komado, E. (1965) Polymorphic transition of FeSiO₃ and CoSiO₃ at high pressures and temperatures. *Journal of Geophysical Research*, 70, 5269-5278.
- Amthauer, G., Annersten, H., and Hafner, S.S. (1976) The Mössbauer spectrum of ⁵⁷Fe in silicate garnets. *Zeitschrift für Kristallographie*, 143, 14-55.

- Bohlen, S.R., and Boettcher, A.L. (1982) The quartz = coesite transformation: A precise determination and the effects of other components. *Journal of Geophysical Research*, 87, 7073–7078.
- Bohlen, S.R., Essene, E.J., and Boettcher, A.L. (1980) Reinvestigation and application of olivine-quartz-orthopyroxene barometry. *Earth and Planetary Science Letters*, 47, 1–10.
- Bohlen, S.R., Dollase, W.D., and Wall, V.J. (1983a) Calibration and applications of spinel equilibria in the system FeO-Al₂O₃-SiO₂. *Journal of Petrology*, 27, 1143–1156.
- Bohlen, S.R., Wall, V.J., and Boettcher, A.L. (1983b) Experimental investigations and geological applications of equilibria in the system FeO-TiO₂-Al₂O₃-SiO₂-H₂O. *American Mineralogist*, 68, 1049–1058.
- Cressey, G., Schmid, R., and Wood, B.J. (1978) Thermodynamic properties of almandine-grossular garnet solid solutions. *Contributions to Mineralogy and Petrology*, 67, 397–404.
- Geiger, C.A., Newton, R.C., and Kleppa, O.J. (1987) Enthalpy of mixing of synthetic almandine-grossular and almandine-pyrope garnets from high temperature solution calorimetry. *Geochimica et Cosmochimica Acta*, 51, 1755–1763.
- Geiger, C.A., Rubie, D.C., Ross, C.R., II, and Seifert, F. (1991) A cation partitioning study of (Mg,Fe)SiO₃ garnet using ⁵⁷Fe Mössbauer spectroscopy. *Eos*, 72, 564–565.
- Hackler, R.T., and Wood, B.J. (1989) Experimental determination of Fe and Mg exchange between garnet and olivine and estimation of Fe-Mg mixing properties in garnet. *American Mineralogist*, 74, 994–999.
- Hawthorne, F.C. (1981) Some systematics of the garnet structure. *Journal of Solid State Chemistry*, 37, 157–164.
- Hensen, B.J. (1970) Experimental determination of the stability of cordierite and garnet in pelitic compositions and high pressures and temperatures. Ph.D. thesis, Australian National University, Canberra.
- Holland, T.J.B. (1980) The reaction albite = jadeite + quartz determined experimentally in the range 600–1200 °C. *American Mineralogist*, 65, 129–134.
- Holland, T.J.B., and Powell, R. (1990) An enlarged and updated internally consistent thermodynamic dataset with uncertainties and correlations: The system K₂O-Na₂O-CaO-MgO-MnO-FeO-Fe₂O₃-Al₂O₃-TiO₂-SiO₂-C-H₂-O₂. *Journal of Metamorphic Petrology*, 8, 89–124.
- Holmes, R.D., O'Neill, H.St.C., and Arculus, R.J. (1986) Standard Gibbs free energy of formation for Cu₂O, NiO, CoO, and Fe₂O: High resolution electrochemical measurements using zirconia solid electrolytes from 900–1400 K. *Geochimica et Cosmochimica Acta*, 50, 2439–2452.
- Hsu, L.C. (1968) Selected phase relationships in the system Al-Mn-Fe-Si-O-H: A model for garnet equilibria. *Journal of Petrology*, 9, 40–83.
- Karpinskaya, T.B., Ostrovsky, I.A., and Yevstigneeva, T.L. (1982) Synthetic pure iron skiaegite garnet. *Izvestia Akademii Nauk, SSSR*, 9, 128–129 (in Russian).
- Keesman, I., Matthes, S., Schreyer, W., and Seifert, F. (1971) Stability of almandine in the system FeO-(Fe₂O₃)-Al₂O₃-SiO₂-(H₂O) at elevated pressures. *Contributions to Mineralogy and Petrology*, 31, 132–144.
- Kress, V.C., and Carmichael, I.S.E. (1988) Stoichiometry of the iron oxidation reaction in silicate melts. *American Mineralogist*, 73, 1267–1274.
- Lattard, D., and Schreyer, W. (1983) Synthesis and stability of the garnet calderite in the system Fe-Mn-Si-O. *Contributions to Mineralogy and Petrology*, 84, 199–214.
- Lucas, H., Muggerridge, M.T., and McConchie, D.M. (1989) Iron in kimberlitic ilmenites and chromian spinels: A survey of analytical techniques. In J. Ross, Ed., *Kimberlites and related rocks*, vol. 2, p. 311–319. Geological Society of Australia Special Publication, Blackwell, Australia.
- Luth, R.W., Virgo, D., Boyd, F.R., and Wood, B.J. (1990) Ferric iron in mantle-derived garnets, implications for thermobarometry and for the oxidation state of the mantle. *Contributions to Mineralogy and Petrology*, 104, 56–72.
- Massalski, T.B., Murray, J.L., Bennett, L.H., and Baker, H. (1986) Binary alloy phase diagrams, p. 24–26. American Society for Metals, Metals Park, Ohio.
- Meagher, E.P. (1980) Silicate garnets. In *Mineralogical Society of America Reviews in Mineralogy*, 5, 25–66.
- Novak, G.A., and Gibbs, G.V. (1971) The crystal chemistry of the silicate garnets. *American Mineralogist*, 56, 791–825.
- O'Neill, H.St.C. (1987) Quartz-fayalite-iron and quartz-fayalite-magnetite equilibria and the free energy of formation of fayalite (Fe₂SiO₄) and magnetite (Fe₃O₄). *American Mineralogist*, 72, 67–75.
- O'Neill, H.St.C., and Navrotsky, A. (1984) Cation and thermodynamic properties of binary spinel solid solutions. *American Mineralogist*, 68, 181–194.
- O'Neill, H., and Wood, B. (1979) An experimental study of Fe-Mg partitioning between garnet and olivine and its calibration as a geothermometer. *Contributions to Mineralogy and Petrology*, 70, 59–70.
- O'Neill, H.St.C., Rubie, D.C., Canil, D., Geiger, C.A., Ross, C.R., II, Seifert, F., and Woodland, A.B. (1993) Ferric iron in the upper mantle and in transition zone assemblages: Implications for relative oxygen fugacities in the mantle. In E. Takahashi, R. Jeanloz, and D. Rubie, Eds., *Evolution of the Earth and planets: AGU monograph vol. 74 and IUGG vol. 14*, p. 73–88. American Geophysical Union, Washington, DC.
- Paladino, A.E., and Maguire, E.A. (1970) Microstructure development in yttrium iron garnet. *Journal of the American Ceramic Society*, 53, 98–102.
- Ringwood, A.E. (1975) *Composition and petrology of the Earth's mantle*, 618 p. McGraw-Hill, New York.
- Robie, R.A., Hemingway, B.S., and Fisher, J.R. (1978) Thermodynamic properties of minerals and related substances at 298.15 K and 1 bar (10⁵ Pa) pressure and at higher temperature. U.S. Geological Survey Bulletin 1452, 456 p.
- Ross, N., and Navrotsky, A. (1987) The Mg₂GeO₄ olivine-spinel phase transition. *Physics and Chemistry of Minerals*, 14, 473–481.
- Ross, N., Akaogi, M., Navrotsky, A., Susaki, J., and McMillan, P. (1986) Phase transitions among the CaGeO₃ polymorphs (wollastonite, garnet, and perovskite structures): Studies by high pressure synthesis, high temperature calorimetry, and vibrational spectroscopy and calculation. *Journal of Geophysical Research*, 91, 4685–4696.
- Roth, R.S., Dennis, J.R., and McMurdie, H.F. (1987) Phase diagrams for ceramists, vol. VI, p. 454–456. American Ceramic Society, Westerville, Ohio.
- Rubinstein, C.B., and Barns, R.L. (1964) Crystallographic data for rare-earth aluminum garnets. *American Mineralogist*, 49, 1489–1490.
- Schreyer, W., and Baller, Th. (1980) Calderite, Mn³⁺Fe³⁺Si₂O₁₂, a high pressure garnet. *Proceedings of the IMA Meeting, Experimental Mineralogy*, 16, 68–77.
- Shannon, R.D. (1976) Revised effective ionic radii and systematic studies of interatomic distances in halides and chalcogenides. *Acta Crystallographica*, A32, 751–767.
- Stadnik, Z.M. (1984) Electric field gradient calculations in rare-earth iron garnets. *Journal of Physics and Chemistry of Solids*, 45, 311–318.
- Wood, B.J., Bryndzia, L.T., and Johnson, K.E. (1990) Mantle oxidation state and its relation to tectonic environment. *Science*, 248, 337–345.
- Woodland, A.B., and Wood, B.J. (1989) Electrochemical measurement of the free energy of almandine (Fe³⁺Al₂Si₃O₁₂) garnet. *Geochimica et Cosmochimica Acta*, 53, 2277–2282.
- Yagi, T., and Akimoto, S. (1976) Direct determination of coesite-stishovite transition by in-situ X-ray measurements. *Tectonophysics*, 35, 259–270.
- Yagi, T., Akaogi, M., Shimomura, O., Suzuki, T., and Akimoto, S. (1987) In-situ observation of the olivine spinel transformation in Fe₂SiO₄ using synchrotron radiation. *Journal of Geophysical Research*, 92, 6207–6213.
- Yoder, H.S., and Keith, M.L. (1951) Complete substitution of aluminum for silicon: The system 3MnO·Al₂O₃·3SiO₂·3Y₂O₃·5Al₂O₃. *American Mineralogist*, 36, 519–533.